Initial Result of Successive SXR Imaging Measurement in Low-*A* RFP*)

Akio SANPEI, Kensuke OKI, Mitsuru NAKAMURA, Akio HIGASHI, Hidehiko MOTOI, Daisuke FUKAHORI, Haruhiko HIMURA, Sadao MASAMUNE, Satoshi OHDACHI[1)], Nobuhiro NISHINO[2)], Takumi ONCHI[3)] and Ryuya IKEZOE[4)]

Kyoto Institute of Technology, Matsugasaki, Sakyo-ku, Kyoto 606-8585, Japan
[1)]*National Institute for Fusion Science, Oroshi-cho, Toki 509-5292, Japan*
[2)]*Hiroshima University, Hiroshima 739-8527, Japan*
[3)]*University of Saskatchewan, Saskatchewan S7N 5E2, Canada*
[4)]*University of Tsukuba, Tsukuba, Ibaraki 305-8577, Japan*

(Received 7 December 2010 / Accepted 7 April 2011)

A fast successive soft-X ray (SXR) imaging system where SXR camera and high-speed camera for the study of time evolution of magnetic islands has been constructed. A preliminary experimental result in which we observed tangential SXR images from quasi-periodic quasi-single helicity (QSH) state in low-aspect-ratio (low-*A*) reversed field pinch (RFP) is presented. We successfully obtained time evolution of SXR images from tangential port. By comparison obtained images with simulated images, we may conclude that the evolution of experimental SXR image suggests the rotating QSH RFP configuration. The filamentous configuration tends to be observed in QSH state rather than in multi-helicity (MH) state.

Keywords: RFP, soft-X ray (SXR), imaging, magnetic island, high-speed camera

DOI: 10.1585/pfr.6.2406096

1. Introduction

Soft-X ray (SXR) emissivity measurements are often adopted for studies of both equilibrium and fluctuation structures in combination with computer tomography (CT) techniques. Tangential SXR imaging has been applied to high-temperature toroidal plasma experiments for the study of fluctuations either in the core or at the edge [1]. Moreover, fast successive imaging measurement has been a useful tool to understand many aspects of plasma research involving dynamic plasma formation processes, plasma equilibria, magnetic reconnection, or plasma instabilities [2, 3].

Three-dimensional (3-D) structural studies are of crucial importance for toroidal confinement systems. In addition to the conventional asymmetric toroidal systems such as stellarator/heliotron plasmas, 3-D effects in axisymmetric systems such as tokamaks and/or reversed field pinches (RFPs) have attracted much attention. In the RFP, for example, recent progress have shown the importance of helically deformed RFP configuration where single helical magnetic axis state is self-organized [4]. Since the internally resonant single tearing mode causes helical deformation of RFP, development of imaging diagnostics for magnetic islands structure is required for the detailed study on dynamics of the self-organizing process. We have proposed SXR imaging diagnostics using SXR camera for the identification of local structures of dominant MHD instabilities in the RFP [5, 6]. Detailed design of SXR imaging system from low-aspect-ratio (low-*A*) RFP machine REversed field pinch of Low Aspect eXperiment (RELAX) [7, 8], device with $R = 0.51$ m / $a = 0.25$ m ($A = 2$), where R is the major radius and a is the minor radius, has been reported in Ref. [9]. In the present study, we are developing a fast successive SXR imaging system where SXR camera and high-speed camera for the study of time evolution of magnetic island in RFP. As a preliminary experiment, we have taken tangential SXR pin-hole pictures with time resolution of 10 μsec, to identify time evolution of filament-like single helix structure in RELAX plasmas.

In this paper, we describe the arrangement of the successive SXR imaging system. A preliminary experimental result obtained from tangential port will be presented. Then, we compare the obtained images with simulated images. Finally, relation between singularity of mode and filament configuration will be presented.

2. Experimental Set-up and Results

In order to study of time evolution of magnetic island structure, successive SXR imaging system with high time

author's e-mail: sanpei@kit.ac.jp
*) This article is based on the presentation at the 20th International Toki Conference (ITC20).

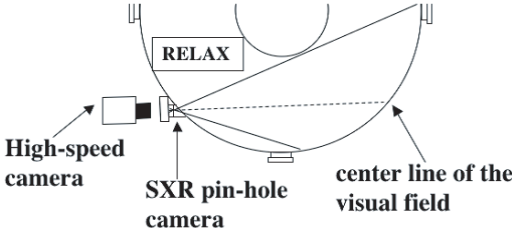

Fig. 1 Arrangement of the SXR pin-hole camera and the high-speed camera. Solid lines and a dashed line represent the limits of the visual field and the line sight of the center of the visual field, respectively.

resolution is being constructed. A schematic drawing of the developing imaging system is illustrated in Fig. 1. Plural unit is located tangential view of the plasma to have a view of nearly the entire plasma diameter and most of the vertical extent of the plasma. Solid lines and a dashed line represent the limits of the visual field and the line sight of the center of the visual field, respectively. This SXR imaging system utilizes a microchannel plate (MCP) to record a higher-resolution distribution of two-dimensional (2-D) luminosity on a phosphor plate. The projected images strongly depend on the equilibrium magnetic field. Clarifying a correlation between the high toroidal mode number n filament structure and a projected tangential image is difficult. As the A of RFP is lowered, the safety factor q on axis increases and n of dominant internally resonant mode is to be lower. In this sense, the core of a low-A RFP is favorable for this kind of tangential measurement.

To determine whether SXR images with high-speed camera can be obtained in RELAX, we have conducted an test experiment. In low-A RFP machine RELAX, a quasi-periodic transition to a quasi-single helicity (QSH) state in which the internally resonant single tearing mode grows significantly larger than other modes state has been observed [10]. During the QSH state, the fluctuation power is concentrated to the single dominant $m = 1$ mode. Figure 2 (a) shows the time evolution of the amplitudes of $m = 1/n = 3, 4, 5$ modes with an expanded time scale. In this shot, dominant mode changes as time goes. The $m = 1/n = 3$ mode grows from 1.31 ms for about 0.01 ms, and then a gradual decay follows. From 1.39 ms, on the other hand, the $m = 1/n = 5$ mode growth and decay is observed. Similar quasi-periodic growth and decay of the dominant $m = 1$ mode continues to the end of the loss of field reversal. There appears to be a trend that these neighboring modes grow (decay) during the decaying (growing) phase of the dominant $m = 1$ mode. In Fig. 2 (b), we compare the time evolution of the phase of the $m = 1/n = 5$ mode to that of the $m = 1/n = 3, 4$ mode. A correlation is indicated between the quasi-periodic oscillation of the mode amplitude and phase evolution. During the growth of either mode, the phase of the corresponding mode does not change much, whereas the phase changes rapidly during the decay of the corresponding mode.

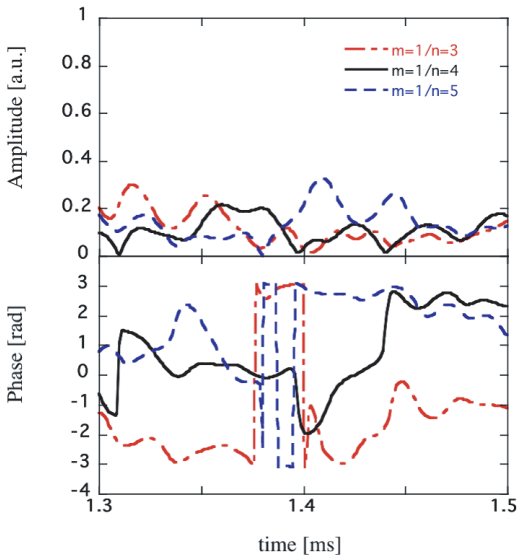

Fig. 2 Time evolution of the amplitude in $m = 1/n = 3, 4, 5$ modes (a), the phase of the $m = 1/n = 3, 4, 5$ modes (b).

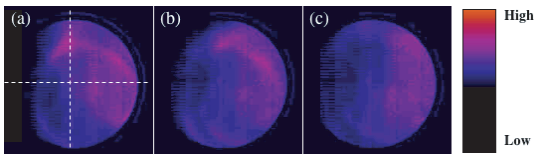

Fig. 3 Snapshots of time evolution of obtained tangential SXR images during QSH RFP state at (a) 1.39 ms (b) 1.40 ms (c) 1.41 ms. Dashed lines in (a) represent the axis of view field.

In this preliminary experiment, we have taken tangential SXR pin-home pictures with time resolution of 10 μ sec, to identify time evolution of filament-like single helix structure in quasi-periodic QSH state in the RELAX plasmas. Here, we show a preliminary experimental result in which we observed tangential SXR images from QSH RFP discharges correspond to Fig. 2. 2-D luminosity distributions corresponding to integrated SXR emissivity are measured with a high-speed camera (Photoron FASTCAM SA-4) with an image size of 320×192 pixels array and 12 bits of dynamic range. Figure 3 shows snapshots of obtained tangential SXR images with developed SXR diagnostic system at from 1.39 ms to 1.41 ms after plasma ignition, i.e. Fig. 3 was taken at QSH state. In Fig. 3 (a), luminosity distribution like as a tip of arrow is observed in upper of figure. And filament structure is also observed in upper right of figure. Comparing with each figures, it is recognized that these structures move to the right direction as time goes. We successfully obtained time evolution of SXR images from tangential port and these figures may reflect the configuration of rotating QSH.

3. Calculated 2-D SXR Images

We have calculated SXR images for some model profiles of SXR emissivity to make clear the meaning of the configuration in 2-D SXR images such as Fig. 3. Images of SXR emission contain both from equilibrium component and from fluctuation component. In the calculation, equilibrium component of SXR emissivity is decided with equilibrium reconstruction from several external diagnostics on RELAX, plasma current I_p, average toroidal field $<B_\phi>$, edge toroidal and poloidal field $B_\phi(a)$, $B_\theta(a)$ and internal line-averaged density n_e obtained with interferometer [11]. Edge magnetic measurement decides size and phase of magnetic islands. The magnetic island width W due to the corresponding m/n tearing mode can be estimated as

$$W = 4r_{mn}\left[\frac{B_r^1}{mB_\theta}\left(\frac{q}{rq'}\right)\Big|_{r_{mn}}\right]^{1/2}, \quad (1)$$

where B_r^1 is the fluctuation component of B_r for the corresponding tearing mode. When the W of neighboring islands are sufficiently broad, they are overlapped each other, resulting in a stochastic magnetic field. Rational surface is also obtained with equilibrium reconstruction. We have already simulated the SXR image obtained from tangential SXR camera in low-A [9].

In this calculation, we assume the constant radiation along the magnetic field line. Phase of magnetic island ϕ is fixed with experimental data obtained with edge magnetic measurement. SXR emissivity profiles are controllable without departing from the result of equilibrium reconstruction. The spatial structure of the SXR emission profile has been assumed as follows. As a background SXR emissivity profile, we have used a broad profile consistent with the features of the result of equilibrium reconstruction from experimental result. The emissivity power is determined as

$$P_{rad} = 1.54\times10^{-32} n_e n_i Z^2 (\kappa T_e)^{1/2}\overline{g_{ff}}(Z, T_e), \quad (2)$$

where n_i is the ion density, Z is the effective ion charge and $\overline{g_{ff}}$ is the temperature averaged free-free Gaunt factor. Here, n_e and n_i are assumed to be equal and Z is unity. Therefore, $P_{rad}(\boldsymbol{r})$ can be decided from $n(\boldsymbol{r})$ and $T_e(\boldsymbol{r})$. Also, as seen from Eq. (2), P_{rad} is proportional to n_e^2 and $T_e^{1/2}$. As a result, the SXR emissivity in the background plasma was assumed to be Gaussian in shape, with FWHM of 17.5 cm (0.7a). The SXR image on the MCP was calculated with by assuming a bean-shaped $m = 1/n = 5$ magnetic island at $r_{s:n=5} = 14$ cm with the normalized width of 12%. The SXR emissivity inside the island was assumed twice as high as that in the background (at the O-point). Figures 4 show the simulated result the SXR image on the MCP calculated with assuming same background SXR distribution and same SXR emissivity inside the island. ϕ is decided by the result of mode analysis from edge magnetic measurements, $\phi = -3.1$ for 1.39 ms (a), $\phi = 2.9$ for 1.40 ms (b) and $\phi = 2.7$ for 1.41 ms (c), respectively. The luminosity distribution like as a tip of arrow and filament similar to the experimental results was reproduced in the calculated images. In this case, there arises a discrepancy in the peak position, however, the overall characteristics show good agreement. The reason of the difference in right edge region is the effect of the Shafranov shift, which is estimated to be about 0.2a from equilibrium reconstruction using the RELAXFit code [11], but not taken into account in calculating the tangential images. In the Figs. 3 (c) and 4 (c), differences become larger because dominant structure is focused in right edge region. From the results in Figs. 3 and 4, we may conclude that the major features of the experimental tangential SXR image could be reproduced by a single island model. Figure 4 represents the rotating QSH configuration, because we assume a single island model and each figures are obtained with change only in ϕ, which are −3.1, 2.9 and 2.7. Therefore, the evolution of experimental SXR image in Figs. 3 may suggests the rotating QSH RFP configuration. It is clear that we need further effort to adjust the island parameters to realize better agreement between the experimental and calculated images. The small-scale structures seen in the experimental images in Fig. 3 may represent the effect of the neighboring modes, which might also have island structures.

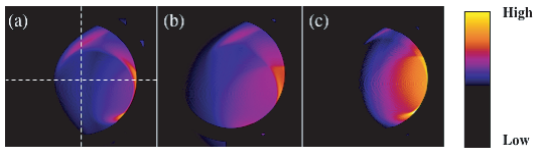

Fig. 4 Simulated tangential SXR images for a single island model. Each figures are corresponding to Figs. 3, respectively. Dashed lines in (a) represent the axis of view field.

4. Discussion and Conclusion

Then, relation between singularity of mode and filament configuration is presented. Figure 5 shows the time evolution of the spectral index N_s defined as

$$N_s = \left[\sum_{n=3}^{8}\left(\frac{b_{1,n}^2}{\Sigma_n b_{1,n}^2}\right)^2\right]^{-1}. \quad (3)$$

When a single mode is excited, N_s becomes 1, while N_s equals the number of the modes considered when all modes have the same magnetic energy. Thus, N_s is often used as an indication of the quality of QSH in RFP. Four pictures around the graph are corresponding experimental images at each times. In above two figures in Figs. 5, it is difficult to determine configurations, such as a tip of arrow and filament, due to multi-helicity (MH) state of plasma. As seen in below two pictures in Figs. 5, on the other hand, we can identify the configuration due to magnetic filament in QSH state. According to mode analysis, the ϕ of $m = 1/n = 5$ in

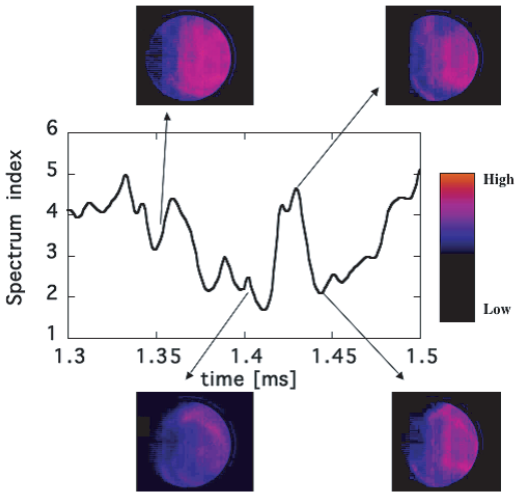

Fig. 5 Relation between singularity of mode and filament configuration.

1.44 ms is similar to its in 1.40 ms. Therefore, the luminosity distribution seems to be similar tendency with each other. Figure 5 suggests that luminosity pattern on tangential SXR image being consistent with the edge magnetic measurement. Moreover, coming and going of filamentous configuration reflects the realization of quasi-periodic QSH RFP state. More detailed analysis is in progress.

In conclusion, initial result of successive SXR imaging measurement with high-speed camera has been presented. We show a preliminary experimental result in which we observed tangential SXR images from quasi-periodic QSH RFP state. We successfully obtained time evolution of SXR images from tangential port. We have calculated SXR images for some model profiles of SXR emissivity to make clear the meaning of the configuration in 2-D SXR images. By comparison obtained experimental images during single mode dominant phase with simulated SXR images calculated on the assuming rotating QSH configuration, we may conclude that the evolution of experimental SXR image suggests the rotating QSH RFP configuration. The relation between singularity of mode and filament configuration has been presented. The filamentous configuration tends to be observed in QSH state rather than in MH state. We need further elaboration of the imaging diagnostics to identify whether the shape of the helical structure is magnetic island or helically deformed 3-D magnetic axis configuration.

Acknowledgements

This study is supported by a U.S.-Japan collaboration and by a Grant-in-Aid for Scientific Research (No.17360441) from the Ministry of Education, Culture, Sports and Technology, Japan. The study is performed with the support and under the auspices of the National Institute for Fusion Science (NIFS) Collaborative Research Program (NIFS10KOAP024).

[1] S. Ohdachi *et al*., Plasma Fusion Res. **2**, S1016 (2007).
[2] N. Nishino *et al*., Plasma Fusion Res. **1**, 035 (2006).
[3] U. Shumlak *et al*., Nucl. Fusion **49**, 0750039 (2009).
[4] R. Lorenzini *et al*., Nature Phys. **5**, 570 (2009).
[5] A. Sanpei *et al*., Plasma Fusion Res. **2**, S1064 (2007).
[6] T. Onchi *et al*., Plasma Fusion Res. **2**, S1063 (2007).
[7] S. Masamune *et al*., J. Phys. Soc. Jpn. **76**, 123501 (2007).
[8] K. Oki *et al*., J. Phys. Soc. Jpn. **77**, 075005 (2008).
[9] T. Onchi *et al*., Rev. Sci. Instrum. **81**, 073502 (2010).
[10] R. Ikezoe *et al*., Plasma Fusion Res. **3**, 029 (2008).
[11] A. Sanpei *et al*., J. Phys. Soc. Jpn. **78**, 013501 (2009).